

Tetragonal $\text{Li}_{10}\text{GeP}_2\text{S}_{12}$ and Li_7GePS_8 – exploring the Li ion dynamics in LGPS Li electrolytes†Cite this: *Energy Environ. Sci.*, 2013, **6**, 3548Alexander Kuhn,^a Viola Duppel^a and Bettina V. Lotsch^{*ab}Received 21st May 2013
Accepted 4th October 2013

DOI: 10.1039/c3ee41728j

www.rsc.org/ees

Tetragonal $\text{Li}_{10}\text{GeP}_2\text{S}_{12}$ (LGPS) is the best solid Li electrolyte reported in the literature. In this study we present the first in-depth study on the structure and Li ion dynamics of this structure type. We prepared two different tetragonal LGPS samples, $\text{Li}_{10}\text{GeP}_2\text{S}_{12}$ and the new compound Li_7GePS_8 . The Li ion dynamics and the structure of these materials were characterized using a multitude of complementary techniques, including impedance spectroscopy, ^7Li PFG NMR, ^7Li NMR relaxometry, X-ray diffraction, electron diffraction, and ^{31}P MAS NMR. The exceptionally high ionic conductivity of tetragonal LGPS of $\sim 10^{-2} \text{ S cm}^{-1}$ is traced back to nearly isotropic Li hopping processes in the bulk lattice of LGPS with $E_A \approx 0.22 \text{ eV}$.

Lithium-ion batteries are considered to play an important role in future energy storage, especially for mobile applications such as vehicle propulsion.¹ One approach to overcome both safety and durability problems of state-of-the-art Lithium-ion batteries is the use of solid electrolytes, which must satisfy the criteria of having high Li ion conductivity and a wide electrochemical window. The lack of suitable materials triggered intense research efforts in the field of solid state ionics. During recent years significant progress has been achieved, such that the materials available now are suitable for commercial applications.² Hereby, two main classes of solid electrolytes have attracted the attention of both academia and industry, namely (i) oxide-based garnet-type electrolytes such as $\text{Li}_7\text{La}_3\text{Zr}_2\text{O}_{12}$,^{3–5} and (ii) sulfide-based electrolytes.^{6–8} The oxide-based materials generally show a wider electrochemical window, whereas the sulfide-based electrolytes usually exhibit a higher Li-ion conductivity. In 2011, a new solid electrolyte $\text{Li}_{10}\text{GeP}_2\text{S}_{12}$ (LGPS), a metastable phase occurring in the system $x\text{Li}_4\text{GeS}_4:y\text{Li}_3\text{PS}_4$, was reported.⁹ Tetragonal LGPS combines the most

Broader context

Lithium ion batteries have become key players as highly efficient and practical energy storage systems for mobile applications, especially in vehicle propulsion and portable electronic devices. Current Li-ion battery technology uses Li salts dissolved in organic liquids as electrolytes, which leads to safety issues and limits the cell design to strictly separate cells in a battery stack. In this context, solid electrolytes with Li ion mobilities competitive to those of liquid electrolytes could be advantageous. The lack of a suitable material has triggered intense research during the last decade and several classes of new promising solid electrolytes have since been discovered. A fundamental characterization of the structure and Li ion dynamics of these new materials is crucial for the understanding and further development of next-generation solid electrolytes.

important prerequisites for a high-performance Li electrolyte: a room-temperature conductivity of 12 mS cm^{-1} , an activation energy of 0.24 eV , and an electrochemical window of up to 4 V vs. Li/Li^+ .⁹ While tetragonal LGPS has only been studied by means of MD and *ab initio* calculations since the original publication,^{10–13} a fundamental study on the Li ion dynamics occurring in tetragonal LGPS has not been reported to date. Additionally, the fact that tetragonal LGPS is a solid solution with a rather broad range of existence has not been considered in the literature so far.

In this study, both $\text{Li}_{10}\text{GeP}_2\text{S}_{12}$ and Li_7GePS_8 , a new member of the solid solution of tetragonal LGPS with a Ge : P ratio of 1 : 1, were prepared and structurally characterized. The Li ion dynamics occurring in the materials was studied by several complementary techniques sensitive to (i) long-range Li diffusion (PFG-NMR), (ii) atomic-scale jumps (NMR relaxometry), and (iii) long-range charge transport (impedance spectroscopy). This combination of techniques allows us to connect diffusion (at the macroscopic scale) to ionic hopping in the LGPS lattice (at the microscopic scale). In the studied temperature range between 110 K and 450 K , the Li ion dynamics is well described by an Arrhenius law with an activation energy as low as $0.22(1) \text{ eV}$.

Both Li_7GePS_8 and $\text{Li}_{10}\text{GeP}_2\text{S}_{12}$ were synthesized from stoichiometric amounts of Li_2S , Ge, and P. A slight excess of sulfur

^aMax Planck Institute for Solid State Research, Heisenbergstr. 1, 70569 Stuttgart, Germany. E-mail: b.lotsch@fkf.mpg.de

^bDepartment of Chemistry, Ludwig-Maximilians-Universität München, Butenandtstr. 5–13, 81377 München, Germany

† Electronic supplementary information (ESI) available: See DOI: 10.1039/c3ee41728j

yielding a vapor pressure of approx. 1 bar under the reaction conditions was used in order to ensure complete oxidation of Ge and P. The starting materials were mechanically treated in a high-energy ball mill for 1 day (zirconia vial, Fritsch Premium line 5). The obtained precursor powders were heated in evacuated quartz tubes according to the following temperature programs: Li_7GePS_8 : $30^\circ \text{ h}^{-1} \rightarrow 450^\circ \text{ C}$ (4 h) $\rightarrow 550^\circ \text{ C}$ (1 h); $\text{Li}_{10}\text{GeP}_2\text{S}_{12}$: $30^\circ \text{ h}^{-1} \rightarrow 420^\circ \text{ C}$ (1 d). Due to the lower synthesis temperature $\text{Li}_{10}\text{GeP}_2\text{S}_{12}$ shows a lower crystallinity. However, higher synthesis temperatures for the metastable tetragonal modification unavoidably led to the partial formation of the undesired orthorhombic modification in our experiments.

The products with the composition Li_7GePS_8 and $\text{Li}_{10}\text{GeP}_2\text{S}_{12}$ crystallize in the tetragonal LGPS structure⁹ with $a = b = 8.718(1)$, $c = 12.660(1)$ for Li_7GePS_8 and $a = b = 8.714(2)$, $c = 12.607(3)$ for $\text{Li}_{10}\text{GeP}_2\text{S}_{12}$ (Table 1) as confirmed by X-ray powder diffraction (XRPD, see Fig. 1a), TEM-PED (for Li_7GePS_8 , see Fig. 1b), and single-crystal X-ray diffraction (for $\text{Li}_{10}\text{GeP}_2\text{S}_{12}$, see ref. 15). A Rietveld analysis of the XRPD patterns revealed that Ge and P share the Ge1/P1 position (Wyckoff position: $4d$), while the P2 position (Wyckoff position: $2b$) is solely occupied by P (see ESI† for details of the refinement). The refined occupancy of Ge1/P1 is $0.74(1)/0.26(1)$ for Li_7GePS_8 (theoretical occupancy: $0.75/0.25$), and $0.54/0.46$ for $\text{Li}_{10}\text{GeP}_2\text{S}_{12}$ (theoretical occupancy $0.5/0.5$). This finding was further corroborated by a comparison of the ^{31}P NMR spectra of Li_7GePS_8 and $\text{Li}_{10}\text{GeP}_2\text{S}_{12}$ (Fig. 1C). For Li_7GePS_8 , the area ratio of the two ^{31}P NMR lines associated with tetragonal LGPS is 2 : 1, while for $\text{Li}_{10}\text{GeP}_2\text{S}_{12}$ both lines have the same integral – as expected from the Rietveld refinements of the two compounds. Thus, the solid solution of tetragonal LGPS is best written as $\text{Li}_{11-x}(\text{Ge}_{2-x}\text{P}_x)\text{PS}_{12}$ with the theoretical range of existence $x = 0 \dots 2$. For Li_7GePS_8 , x amounts to 0.5 while for $\text{Li}_{10}\text{GeP}_2\text{S}_{12}$, $x = 1$. Note that both samples carry a low amount of impurities of the orthorhombic modification – observable as a third line in the ^{31}P MAS NMR spectra and, for $\text{Li}_{10}\text{GeP}_2\text{S}_{12}$, in the XRPD pattern. We will discuss possible effects of these impurities on subsequent measurements where appropriate.

In order to probe the Li ion dynamics occurring in Li_7GePS_8 and $\text{Li}_{10}\text{GeP}_2\text{S}_{12}$, Li self-diffusion coefficients D^{tr} were determined using ^7Li PFG NMR. This technique is sensitive to Li ion dynamics on a macroscopic (μm) scale and insensitive to less conductive impurities. The Li self-diffusion coefficients D^{tr} shown in Fig. 2B for Li_7GePS_8 (grey squares) and $\text{Li}_{10}\text{GeP}_2\text{S}_{12}$ (red triangles) were extracted from the attenuation of the stimulated echo (see Fig. 2A) using the Stejskal–Tanner

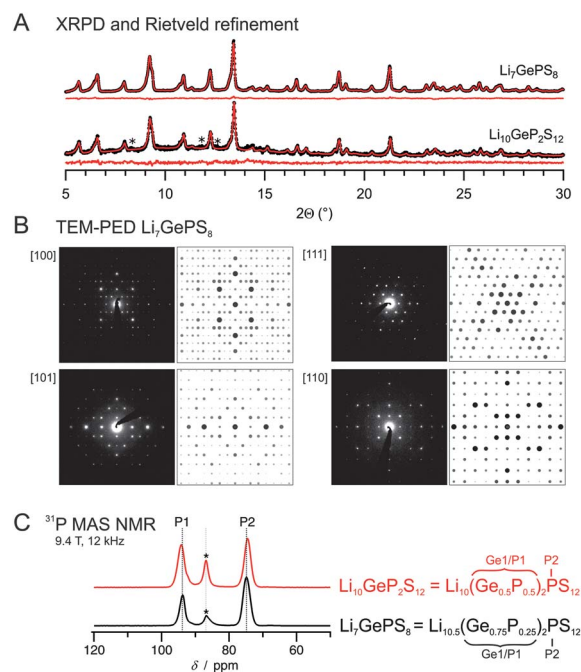


Fig. 1 Structural characterization of Li_7GePS_8 and $\text{Li}_{10}\text{GeP}_2\text{S}_{12}$. (A): XRPD patterns with single-phase Rietveld refinement. The asterisks denote reflections of the orthorhombic modification (side phase). (B): measured (left) and simulated¹⁴ (right) TEM precession electron diffraction (PED) patterns of Li_7GePS_8 for selected orientations. (C): ^{31}P MAS NMR spectra of Li_7GePS_8 and $\text{Li}_{10}\text{GeP}_2\text{S}_{12}$. The asterisk denotes the ^{31}P signal of a minority phase, probably pertaining to the orthorhombic modification of LGPS with low crystallinity. The assignment of the chemical shift was confirmed with an LGPS sample showing the orthorhombic modification.

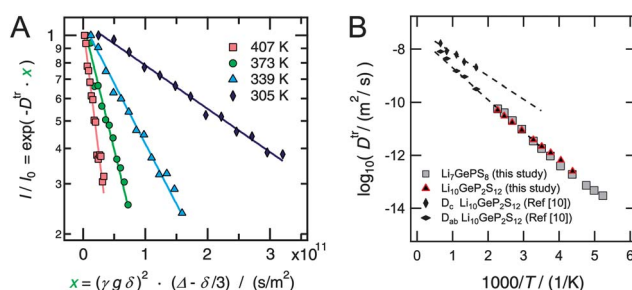


Fig. 2 ^7Li PFG NMR on Li_7GePS_8 and $\text{Li}_{10}\text{GeP}_2\text{S}_{12}$. (A): echo attenuation curves for selected temperatures (Li_7GePS_8). (B): tracer diffusion coefficients extracted from the echo attenuation. At all temperatures, the diffusion time Δ was set short enough to avoid finite crystallite size effects (cf. ESI†).

Table 1 Crystallographic details of Li_7GePS_8 and $\text{Li}_{10}\text{GeP}_2\text{S}_{12}$

	Li_7GePS_8	$\text{Li}_{10}\text{GeP}_2\text{S}_{12}$
Space group	$P4_2/nmc$ (137 : 1)	$P4_2/nmc$ (137 : 1)
Lattice constants	$a = b = 8.718(1) \text{ \AA}$ $c = 12.660(1) \text{ \AA}$	$a = b = 8.714(2) \text{ \AA}$ $c = 12.607(3) \text{ \AA}$
Refined occupancy		
Ge1/P1 ($4d$ site)	$0.74(1)/0.26(1)$	$0.54(2)/0.46(2)$
P2 ($2b$ site)	P only	P only

equation for 3D isotropic diffusion.¹⁶ Note that we do not find a significant deviation from that behaviour in our measurements. The so-obtained self-diffusion coefficients are activated with $0.23(1)$ eV for Li_7GePS_8 and with $0.21(1)$ eV for $\text{Li}_{10}\text{GeP}_2\text{S}_{12}$. Obviously, the Li diffusivity is rather insensitive to the Ge/P ratio within the considered compositional range. For comparison, the theoretical diffusion coefficients along the c -axis D_c and in the ab -plane D_{ab} as obtained from a DFT MD simulation reported by Mo *et al.*¹⁰ are included in Fig. 2B. Here, a strong anisotropy of the Li diffusivity for $\text{Li}_{10}\text{GeP}_2\text{S}_{12}$ was suggested. In fact, there is no sign of the predicted ultrafast diffusion process

along the *c*-axis (see Fig. 2B) in our PFG NMR measurements, *i.e.* it does not contribute to long-range Li transport on the micron scale. However, there is an excellent agreement of the extrapolated experimental diffusivities D^{tr} and the simulated diffusivities in the *ab*-plane D_{ab} .¹⁰

This finding is consistent with the assumption that for a true single-file 1D Li ion conductor, the macroscopic Li self-diffusion coefficient should be zero since Li ions cannot pass one another and a strictly unidirectional drift of Li ions is not allowed for reasons of charge separation. Accordingly, for a quasi-1D conductor, the self-diffusivity along the *c*-axis should be limited by the diffusivity in the *ab*-plane, thus leading to quasi-isotropic self-diffusion. In line with these considerations, the experimental 3D self-diffusion coefficients D^{tr} fit very well to the diffusion coefficients in the *ab*-plane D_{ab} obtained in the theoretical study (see ESI† for further details). In addition to this general argument, 1D diffusion is especially susceptible to blocking defects in real-world materials as also pointed out by Mo *et al.*¹⁰

For a fundamental understanding of the Li diffusion in tetragonal LGPS it is crucial to trace back the macroscopic diffusion to its microscopic origin, *i.e.* ionic hopping in the LGPS lattice. This can be achieved with ⁷Li NMR relaxometry.^{17,18} This technique takes advantage of the fact that the hopping process of the ⁷Li spins leads to a fluctuation of the local interaction with their environment. The fluctuation, then, triggers the relaxation. Longitudinal relaxation is sensitive to fast motion occurring on a time scale determined by the Zeeman interaction with the external field (a few hundreds of MHz). In contrast, transversal relaxation can be used to measure much slower dynamics. Here, the window of sensitivity is determined by the internal local interactions, *i.e.* dipolar coupling (a few kHz) and quadrupolar coupling (a few tens of kHz), respectively. The results of the NMR relaxometry study are summarized in Fig. 3. Transversal relaxation can simply be measured as the static ⁷Li NMR line. Fig. 3A shows the temperature-dependent NMR line of Li₇GePS₈ (left) and Li₁₀GeP₂S₁₂ (right) as measured with single-pulse excitation. At very low temperatures, in the so-called rigid lattice regime – here below $T_{\text{onset}} \approx 135$ K – the line is broad and Gaussian-shaped due to the dipolar interaction between the ⁷Li nuclei. At higher temperatures, when the mean Li jump rate exceeds the rigid-lattice linewidth, the line narrows successively. Fig. 3D shows the motional narrowing curves of the ⁷Li NMR central transition, which are identical for Li₇GePS₈ and Li₁₀GeP₂S₁₂ within the accuracy of the method. Only the rigid lattice linewidth differs slightly, which correlates with the slightly different Li concentration. From the narrowing condition $\tau^{-1} \approx \sqrt{M_2}$ rigid lattice,¹⁷ the Li jump rate at $T_{\text{onset}} \approx 135$ K is obtained as $\tau^{-1} \approx 1.4 \times 10^4$ s⁻¹ for both samples. Hereby, M_2 rigid lattice is Van-Vleck's second moment in the rigid lattice.¹⁹ The so-obtained jump rates are included in the Arrhenius plot of the Li jump rates shown in Fig. 3B. Additionally, T_{onset} can be used to roughly estimate the activation energy of the Li jump process using the empirical formula proposed by Waugh and Fedin,²⁰ $E_A \approx 1.61 \times 10^3 T_{\text{onset}}$ eV K⁻¹. Hereby, an activation energy of 0.22 eV is obtained – in line with the results from PFG NMR. So far, only the central transition was discussed. The quadrupolar structure of the ⁷Li NMR lines representing the satellite

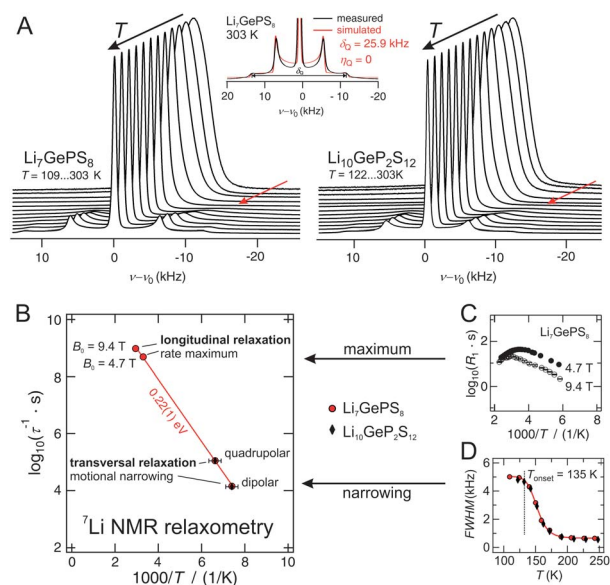


Fig. 3 (A): Temperature-dependent static ⁷Li NMR lines of Li₇GePS₈ (left) and Li₁₀GeP₂S₁₂ (right) measured at 9.4 T. The red arrow indicates the averaging of the static quadrupolar interaction. Inset: measured and simulated²¹ quadrupolar structure of the ⁷Li NMR spectrum of Li₇GePS₈ at 303 K. (B): Arrhenius plot of the jump rates extracted from the NMR relaxometry study. (C) Longitudinal ⁷Li relaxation rates measured at 9.4 T and 4.7 T. (D) Motional narrowing of the FWHM (full width at half maximum) of the central transition of Li₇GePS₈ and Li₁₀GeP₂S₁₂.

transition of the spin-3/2-nuclei is clearly observed only at higher temperatures, while at low temperatures, a very broad Gaussian-shaped feature representing the quadrupolar interaction is observed. This appears much more pronounced in measurements using an echo pulse sequence (not shown). The static quadrupolar interaction averages at temperatures where the jump rate exceeds the time scale of the quadrupolar interaction. Here, from the averaging (marked by red arrows in Fig. 3A), a jump rate of $\tau^{-1} \approx 1.1 \times 10^5$ s⁻¹ at 150 K (included in Fig. 3C) is obtained.

The room-temperature ⁷Li NMR line (enlargement shown for Li₇GePS₈ in the inset of Fig. 3B) shows the typical powder pattern of a spin-3/2-nucleus coupling to an axially symmetric electric field gradient ($\delta_Q = 25.9$ kHz, $\eta_Q = 0$). The fast-diffusing ⁷Li nuclei experience a time average of all site-specific electric field gradients they pass through while diffusing. As expected for a tetragonal crystal system, this average field gradient shows axial symmetry as observed experimentally. This proves that the fast Li reservoir is indeed the Li ions in tetragonal LGPS and not those in a side phase with lower symmetry.

Temperature-dependent longitudinal relaxation rates $R_1(T)$ of Li₇GePS₈ were measured at two different external fields, $B_0 = 4.7$ T and $B_0 = 9.4$ T (see Fig. 3C). $R_1(T)$ passes through a maximum when the Li jump rate fulfils the maximum condition $\tau^{-1} \approx \omega_0 = \gamma B_0$.¹⁷ The two jump rates extracted from the R_1 maxima are included in Fig. 3B (see ESI† for further details).

The jump rates extracted from the NMR relaxometry measurements (transversal and longitudinal relaxation) nicely follow an Arrhenius law with an activation energy of 0.22(1) eV (red regression line) and an attempt frequency of τ^{-1}

$\approx 2 \times 10^{12} \text{ s}^{-1}$. Finally, let us mention that, again, we do not observe the fast jump process expected from MD calculations on the LGPS.^{9–12}

While NMR relaxometry probes Li ion dynamics in the bulk, impedance spectroscopy probes charge transport on different length scales and can be used to study the contributions of the bulk and grain boundary to the overall impedance of the samples. Fig. 4 shows the total impedances (full triangles) and bulk impedances (open triangles) of Li_7GePS_8 and $\text{Li}_{10}\text{GeP}_2\text{S}_{12}$ as measured with impedance spectroscopy. The room temperature conductivity for Li_7GePS_8 and $\text{Li}_{10}\text{GeP}_2\text{S}_{12}$ amounts to 7 mS cm^{-1} and 9 mS cm^{-1} , respectively. For comparison, the reported conductivity for $\text{Li}_{10}\text{GeP}_2\text{S}_{12}$ is also shown (blue dashed line, room temperature conductivity: 12 mS cm^{-1} ; the values correspond to the total impedance).⁹ Again, both samples show very similar behavior.

The total impedance follows a slope of approximately 0.2 eV above room temperature and a slope of 0.3 eV at low temperatures. This points to the presence of blocking grain boundaries (gb) at low temperatures, while at room temperature, the conductivity is unaffected by grain boundary effects. Indeed, using a suitable equivalent circuit, the contributions of bulk, grain boundary, and electrode polarization to the total impedance at low temperatures could be clearly separated (see ESI† for details). The extracted low-temperature bulk impedance and the total impedance at high temperatures together nicely follow an Arrhenius behavior with an activation energy of $0.22(2) \text{ eV}$ – in very good agreement with the results from NMR. The gb contribution, which plays a significant role below 250 K , is activated with $0.30(2) \text{ eV}$.

Taking together the three complementary techniques – PFG NMR (nuclear method, sensitive to long-range Li transport), NMR relaxometry (nuclear method, sensitive to site-to-site hopping of Li), and impedance spectroscopy (non-nuclear method, sensitive to long-range charge transport) – a consistent picture of the Li dynamics in tetragonal LGPS is obtained (see Fig. 5A and B for Li_7GePS_8 and $\text{Li}_{10}\text{GeP}_2\text{S}_{12}$, respectively). Hereby, the Li jump rates τ^{-1} obtained from NMR relaxometry were derived into uncorrelated diffusion coefficients D^{uc} using the Einstein–Smoluchowski equation $D^{\text{uc}} = \frac{a^2}{6} \times \tau^{-1}$ with $a = 2$

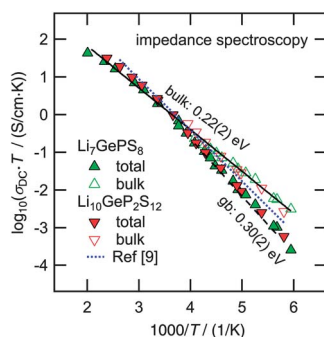


Fig. 4 Impedance spectroscopy: total (full triangles) and bulk (empty triangles) conductivity of $\text{Li}_{10}\text{GeP}_2\text{S}_{12}$ and Li_7GePS_8 . For comparison, the total conductivity reported for $\text{Li}_{10}\text{GeP}_2\text{S}_{12}$ (ref. 9) is included.

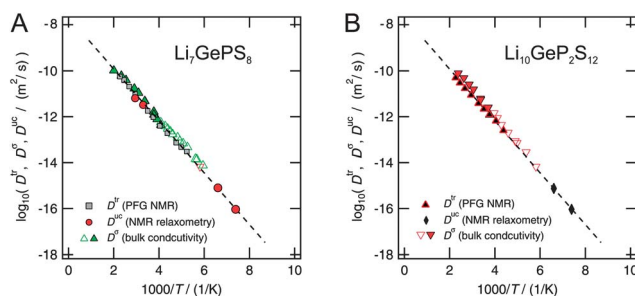


Fig. 5 Comparison of the Li diffusion coefficients obtained from long-range sensitive (PFG NMR, bulk conductivity) and short-range sensitive (NMR relaxometry) methods for Li_7GePS_8 (A) and $\text{Li}_{10}\text{GeP}_2\text{S}_{12}$ (B).

\AA as a mean Li–Li distance. Accordingly, the conductivities σ_{dc} were derived into conductivity diffusion coefficients $D^\sigma = \frac{k_B T}{Nq^2} \times \sigma_{\text{dc}}$ whereby the number density N of the mobile Li ions of charge q was calculated from the crystal structure. The diffusion coefficients obtained from the different methods obviously describe the same process activated by $0.22(2) \text{ eV}$ over a wide temperature range (same dashed line in Fig. 5A and B). Therefore, the bulk conductivity in tetragonal LGPS is unequivocally traced back to its elementary process, being Arrhenius-activated site-to-site hopping of Li ions in the LGPS lattice. The Haven ratio H_R and the correlation factor f which connect D^{tr} with D^{uc} and D^σ according to $D^{\text{tr}} = f \times D^{\text{uc}} = H_R \times D^\sigma$ are both in the order of 1 as expected for simple diffusion mechanisms. The experimental results are in line with the assumption of a nearly isotropic diffusivity.

Conclusions

Tetragonal Li_7GePS_8 and $\text{Li}_{10}\text{GeP}_2\text{S}_{12}$ were synthesized and structurally characterized. The Li ion dynamics of these tetragonal LGPS-type materials was thoroughly characterized and compared with the data available so far. Long-range Li transport, which is relevant for potential applications of these superionic conductors, was traced back to its microscopic origin – Li hopping inside the bulk lattice of the tetragonal structure, activated with 0.22 eV . Both materials show very similar Li diffusivities. We did not observe any signs of a strong anisotropy of the diffusivity in these materials.

Acknowledgements

We thank J. Melchior and K.-D. Kreuer, as well as O. Gerbig and J. Maier for access to the NMR and impedance spectroscopy equipment, respectively. Furthermore, we thank T. Bräuniger for the ^{31}P MAS NMR measurements. We are grateful to C. Schön for valuable discussions and Prof. P. Heitjans for familiarizing A. Kuhn with some of the analytical techniques used in this work, especially NMR relaxometry.

Notes and references

- 1 J.-M. Tarascon and M. Armand, *Nature*, 2001, **414**, 359.

- 2 Toyota prototype all-solid-state battery using $\text{Li}_{10}\text{GeP}_2\text{S}_{12}$, see http://techon.nikkeibp.co.jp/english/NEWS_EN/20120926/241911/.
- 3 R. Murugan, V. Thangadurai and W. Weppner, *Angew. Chem., Int. Ed.*, 2007, **46**, 7778.
- 4 H. Buschmann, J. Dölle, S. Berendts, A. Kuhn, P. Bottke, M. Wilkening, P. Heitjans, A. Senyshyn, H. Ehrenberg, A. Lotnyk, V. Duppel, L. Kienle and J. Janek, *Phys. Chem. Chem. Phys.*, 2011, **13**, 19378.
- 5 M. Kotokubi, H. Munakata, K. Kanamura, Y. Sato and T. Yoshida, *J. Electrochem. Soc.*, 2010, **157**, A1076.
- 6 R. Kanno and M. Murayama, *J. Electrochem. Soc.*, 2001, **148**, A742.
- 7 H. Yamane, M. Shibata, Y. Shimane, T. Junke, Y. Seino, S. Adams, K. Minami, A. Hayashi and M. Tatsumisago, *Solid State Ionics*, 2007, **178**, 1163.
- 8 H.-J. Deiseroth, S.-T. Kong, H. Eckert, J. Vannahme, C. Reiner, T. Zaiss and M. Schlosser, *Angew. Chem., Int. Ed.*, 2008, **120**, 767.
- 9 N. Kayama, K. Homma, Y. Yamakawa, R. Kanno, M. Yonemura, T. Kamiyama, Y. Kato, S. Hama, K. Kawamoto and A. Mitsui, *Nat. Mater.*, 2011, **10**, 682.
- 10 Y. Mo, S. P. Ong and G. Ceder, *Chem. Mater.*, 2012, **24**, 15.
- 11 S. Adams and R. P. Rao, *J. Mater. Chem.*, 2012, **22**, 7687.
- 12 S. P. Ong, Y. Mo, W. D. Richards, L. Miara, H. S. Lee and G. Ceder, *Energy Environ. Sci.*, 2013, **6**, 148.
- 13 M. Xu, J. Ding and E. Ma, *Appl. Phys. Lett.*, 2012, **101**, 031901.
- 14 P. Stadelmann, *Ultramicroscopy*, 1987, **21**, 2.
- 15 A. Kuhn, J. Koehler and B. V. Lotsch, *Phys. Chem. Chem. Phys.*, 2013, **15**, 11620.
- 16 E. O. Stejskal and J. E. Tanner, *J. Chem. Phys.*, 1965, **42**, 288.
- 17 N. Bloembergen, E. M. Purcell and R. V. Pound, *Phys. Rev.*, 1948, **73**, 679.
- 18 A. Kuhn, M. Kunze, P. Sreeraj, H.-D. Wiemhöfer, V. Thangadurai, M. Wilkening and P. Heitjans, *Solid State Nucl. Magn. Reson.*, 2012, **42**, 2.
- 19 J. H. Van Vleck, *Phys. Rev.*, 1948, **74**, 1168.
- 20 J. S. Waugh and I. Fedin, *Soviet Physics – Solid State*, 1963, **4**, 1633.
- 21 *Simulation performed with the WinSolids software*, K. Eichele, Eberhard-Karls-Universität Tübingen, Germany.